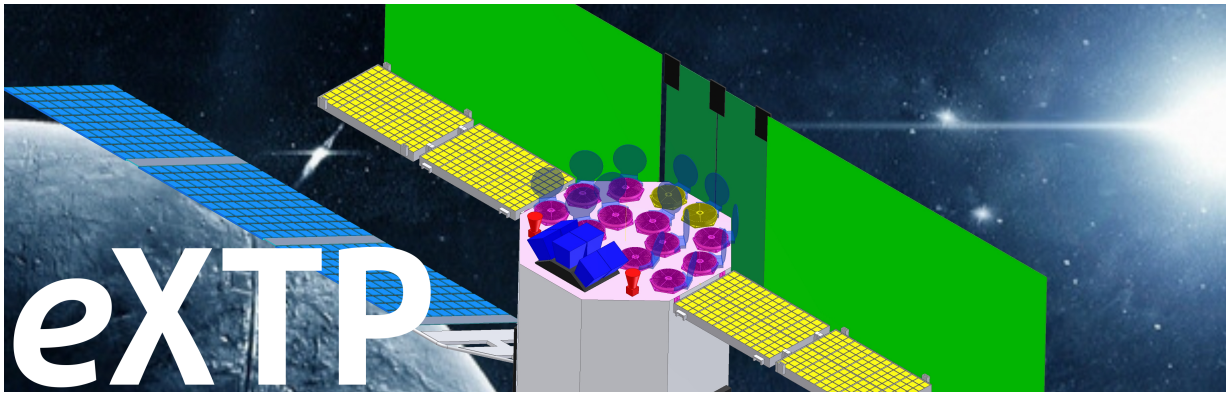


# Dense matter with eXTP

## White Paper in Support of the Mission Concept of the Extended X-ray Timing Polarimetry mission

Authors

**Anna L. Watts**[1], **WenFei Yu**[3], **Juri Poutanen**[4], **Shu Zhang**[2], Alessandro Patruno[5], Ji Long[2], Thomas Riley[1], Sudip Bhattacharyya[8], Slavko Bogdanov[9], Aleksi Kurkela[10], ShuangNan Zhang[2], FangJun Lu[2], RenXin Xu[6], XiangDong Li[7], LiMing Song[2], JinLu Qu[2], MingYu Ge[2], ShiJie Zheng[2]

[1] University of Amsterdam
[2] IHEP
[3] Shanghai Observatory
[4] University of Turku
[5] Leiden Observatory
[6] Beijing University
[7] Nanjing University
[8] Tata Institute of Fundamental Research
[9] Columbia University
[10] CERN

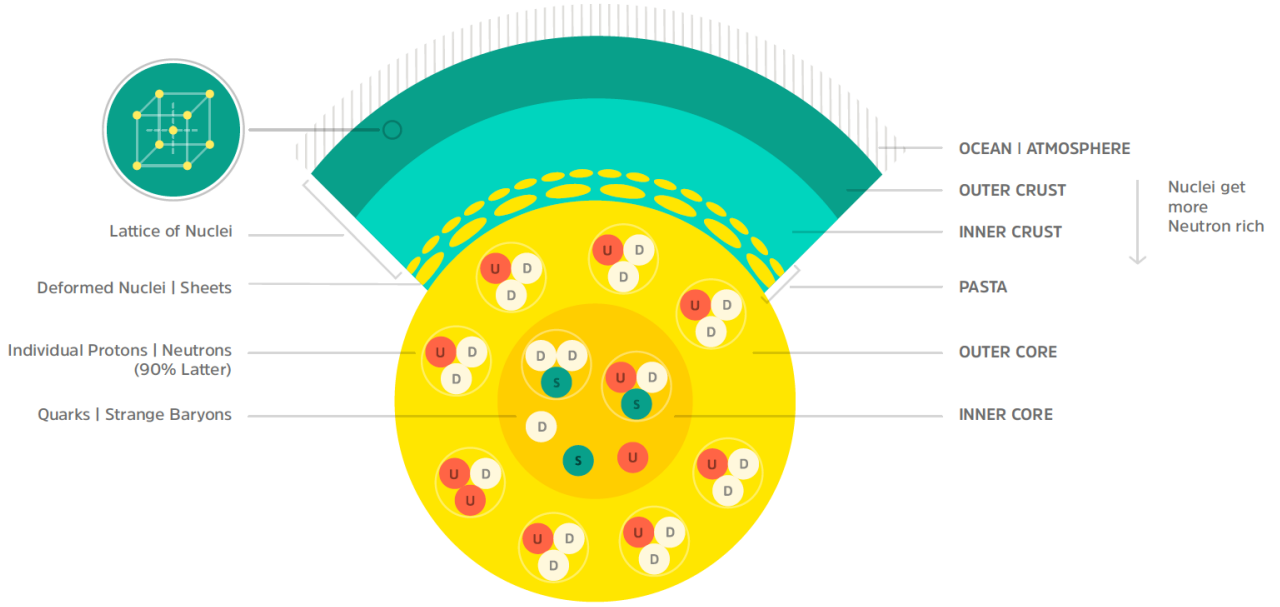


Figure 1: Schematic structure of a neutron star. The outer layer is a solid ionic crust supported by electron degeneracy pressure. Neutrons begin to leak out of ions (nuclei) at densities $\sim 4 \times 10^{11}$ g/cm$^3$ (the neutron drip line, which separates inner from outer crust), where neutron degeneracy also starts to play a role. At the very base of the crust, nuclei may become very deformed (the pasta phase). At densities $\sim 2 \times 10^{14}$ g/cm$^3$, the nuclei dissolve completely and this marks the crust-core boundary. In the core, densities could reach up to ten times the nuclear saturation density of $2.8 \times 10^{14}$ g/cm$^3$ (the density in normal atomic nuclei). The matter in the core is highly neutron-rich, and the inner core may contain stable states of strange matter in deconfined quark or baryonic form. See also Figure 1 of Watts et al. (2016).

## 1 Introduction

One of the overarching goals of modern physics is to understand the nature of the fundamental forces. Here we focus on the strong interaction, which determines the state of nuclear matter and sets the properties of both atomic nuclei and neutron stars, where gravity compresses the material in the core of the star to nuclear densities (Figure 1). The theory of Quantum Chromodynamics, which describes the strong interaction, is however computationally intractable for multi-nucleon systems. Instead, physicists have developed empirical models of nucleonic interactions, which make conflicting predictions. Experiments and observations are vital to test these theories and drive progress.

The quest to test the state of matter under ever more extreme conditions spans the laboratory and the stars (Figure 2). Heavy-ion collision experiments such as ALICE (LHC) or RHIC probe high temperatures and low densities. Neutron stars (NS), by contrast, access a unique regime of parameter space at high density and low temperature. Densities in NS cores can reach $\sim$ 10 times the density of an atomic nucleus, forming states of matter that cannot exist in the laboratory. The low temperatures permit the formation of nuclear superfluids, and the long lifetimes of NS permit long timescale weak interactions to reach equilibrium. This generates matter that is neutron-rich and which may contain deconfined quarks or particles with non-zero net strangeness.

Connecting NS observables to strong interaction physics can be done because the forces between the nuclear particles set the stiffness of neutron star matter. This is encoded in the Equation of State (EOS), the relation between pressure and density. The EOS in turn sets the NS mass M and radius R via the stellar structure equations. By measuring and then inverting the M-R relation, we can recover the EOS (Lindblom, 1992; Özel & Psaltis, 2009, and Figure 3). Measuring the EOS of supranuclear density matter is of major importance to

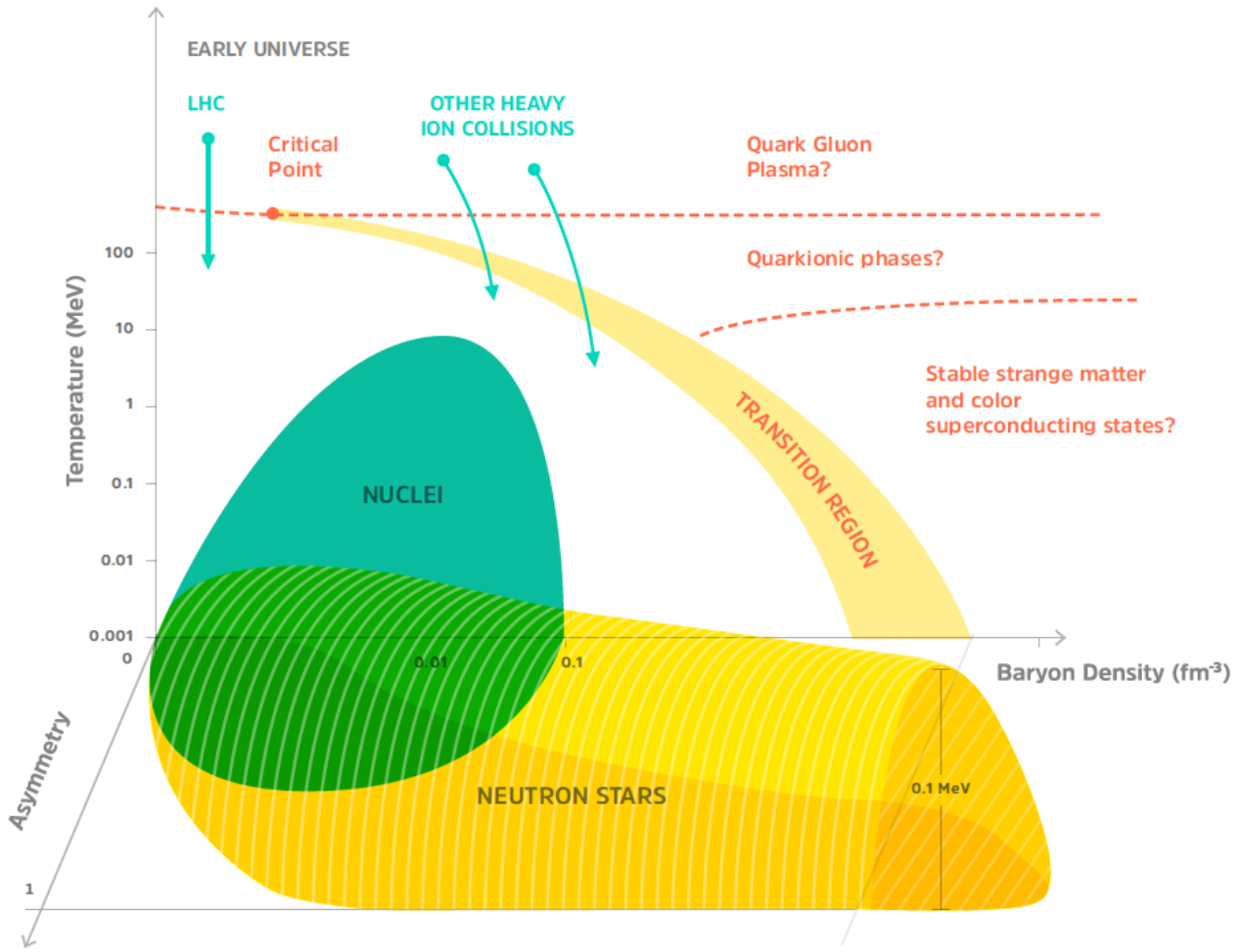


Figure 2: Hypothetical states of matter accessed by NS and current or planned laboratory experiments, in the parameter space of temperature, baryon number density and nuclear asymmetry $\alpha = 1 - 2Y_q$ where $Y_q$ is the hadronic charge fraction ($\alpha = 0$ for matter with equal numbers of neutrons and protons, and $\alpha = 1$ for pure neutron matter). NS access unique states of matter that cannot be created in the laboratory: nuclear superfluids and strange matter states such as hyperons, deconfined quarks, and the color superconductor phase. For simplicity, the transition region is shown only in projection on the density-temperature axis. Figure adapted from Figure 2 of Watts et al. (2015): for an alternative visualisation in the parameter space of temperature and baryon chemical potential, see Figure 2 of Watts et al. (2016).

both fundamental physics and astrophysics. It is central to understanding NS, supernovae, and compact object mergers involving at least one NS (prime gravitational wave sources and the likely engines of short gamma-ray bursts). To distinguish the models shown in Figure 3, one needs to measure M and R to precisions of a few %, for several masses.

Most efforts to date to measure the M-R relation have come from modeling the spectra of thermonuclear X-ray bursts and quiescent low-mass X-ray binaries (Suleimanov et al., 2011a; Özel, 2013; Steiner et al., 2013; Guillot & Rutledge, 2014; Nättilä et al., 2016; Steiner et al., 2017). The constraints obtained so far are weak. The technique also suffers from systematic errors of at least 10% in absolute flux calibration, and uncertainties in atmospheric composition, residual accretion, non-uniform emission, distance, and identification of photospheric touchdown point (Miller, 2013; Poutanen et al., 2014). The planned ESA L-class mission Athena has the right energy band to exploit this technique (Motch et al., 2013): however the systematic uncertainties will remain.

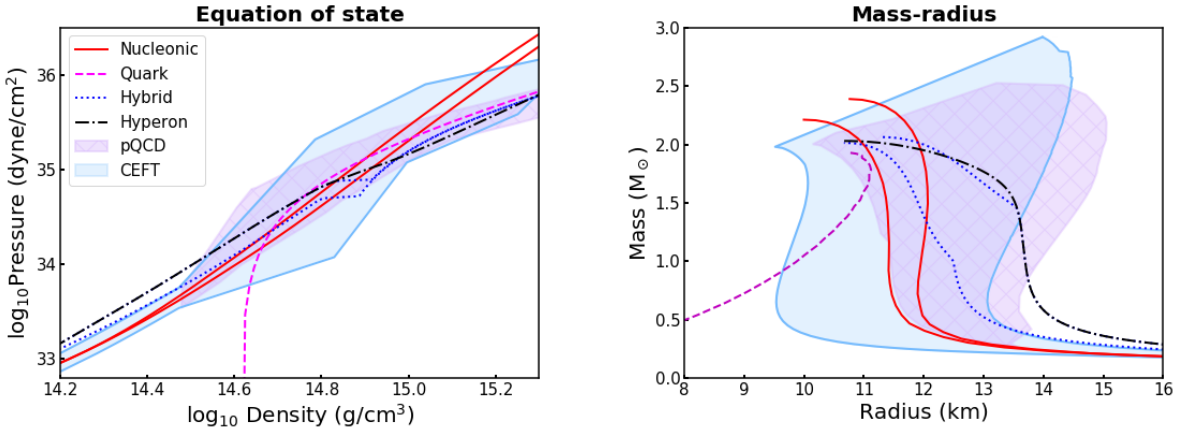


Figure 3: The pressure density relation (EOS, left) and the corresponding M-R relation (right) for some example models with different microphysics. Nucleonic (neutrons, protons): models AP3 and AP4 from Akmal & Pandharipande (1997), also used in Lattimer & Prakash (2001). Quark (u, d, s quarks): model SQM3 from Prakash et al. (1995), also used in Lattimer & Prakash (2001). Hybrid (inner core of uds quarks, outer core of nucleonic matter): models from Zdunik & Haensel (2013). Hyperon (inner core of hyperons, outer core of nucleonic matter): Model from Bednarek et al. (2012). CEFT: range of nucleonic EOS based on chiral effective field theory from Hebeler et al. (2013). pQCD: range of nucleonic EOS from Kurkela et al. (2014) that match to perturbative QCD (pQCD) calculations at higher densities than shown in this figure.

The X-ray timing instrument NICER (Arzoumanian et al., 2014), which was installed on the International Space Station in 2017 and which will instead use the pulse-profile modelling technique, is discussed in more detail in Section 2.4.

Constraints have also come from radio pulsar timing, where the masses of NS in compact binaries can be measured very precisely: high mass stars give the strongest constraint on the EOS. However even the discovery of pulsars with masses $\approx 2M_{\odot}$ (Demorest et al., 2010; Antoniadis et al., 2013), has left a broad range of EOS viable. The next generation of radio telescopes (the Square Kilometer Array and its precursors) will deliver improved mass measurements. Precision radius measurements, however, will be more challenging: there is only one source, the Double Pulsar, for which we expect a radius measurement with 5% accuracy (via its moment of inertia) within the next 20 years (Kramer & Wex, 2009; Watts et al., 2015).

Following paragraph currently based on the rumours: will update once LIGO's paper is available.

The gravitational wave telescopes Advanced LIGO (The LIGO Scientific Collaboration et al., 2015) and Advanced VIRGO (Acernese et al., 2015), have now made the first direct detection of a binary neutron star merger. Gravitational waves from the late inspirals of binary neutron stars are sensitive to the EOS, with departures from the point particle waveform due to tidal deformation constraining M and R (Read et al., 2009). In the event of a very high signal to noise signal, Advanced LIGO/VIRGO may be able to constrain R to $\sim$ 10 % (Read et al., 2013; Hotokezaka et al., 2016). More realistic estimates indicate a few tens of detections are likely to be required to reach this level of accuracy (Del Pozzo et al., 2013; Agathos et al., 2015; Lackey & Wade, 2015; Chatziioannou et al., 2015). There may also be systematic errors of comparable size due to approximations made or higher order terms neglected in the templates (Favata, 2014; Lackey & Wade, 2015). The coalescence can also excite post-ringdown oscillations in the supermassive neutron star remnant that may exist very briefly before collapse to a black hole. These oscillations are sensitive to the finite temperature EOS (Bauswein et al., 2012, 2014; Takami et al., 2014), but detection will be difficult because there are no complete waveform models for the pre and post merger signal (Clark et al., 2016). The eventual detection of NS-black hole binary mergers may also yield EOS constraints (see for example Lackey et al., 2014).

## 2 Pulse profile modelling

### 2.1 Basic principles of pulse profile modeling

Pulse profile modeling exploits localised, radiatively intense regions (hereafter 'hot-spots') that can develop on the NS (the physical motivation and scope of such a model will be outlined in subsequent sections). As the star rotates, a hot-spot gives rise to an observable pulsation in the X-ray. Prior to observation, the photons propagate through the curved exterior spacetime of the spinning compact star. Extensive work on propagation of electromagnetic radiation through such spacetimes has now quantified fully the relativistic effects on the photons, and thus on the pulse profile(Pechenick et al., 1983; Miller & Lamb, 1998; Poutanen & Gierliński, 2003; Poutanen & Beloborodov, 2006; Cadeau et al., 2007; Morsink et al., 2007; Bauböck et al., 2013; Psaltis & Özel, 2014); the simulations in Figure 4 illustrate such observables.

We now describe in a simplified manner how several of these effects encode information on M and R. General relativistic (hereafter GR) light-bending, which is highly sensitive to compactness M/R in the near vicinity of the NS, directly affects both the amplitude of the pulsations and photon time-delays from distinct points on the NS surface. Gravitational redshifting of photons is also entirely dependent on the compactness, and manifests principally in the energy-dependent normalisation of the pulse profile. Relativistic beaming introduces asymmetry and harmonic content in the pulse profile; locally, beaming depends on the projected velocity of the (relativistically moving) hot-spot along a light-ray connecting a point on the local NS surface to the observer. The functional form of the local speed contains R and the (coordinate) angular velocity of the rigidly rotating star; these two parameters are degenerate with respect to local beaming. However, the stellar angular velocity can be accurately measured from the observed pulse frequency, and thus indirectly provides a constraint on R by breaking this degeneracy. Figure 5 demonstrates sensitivity of the observable to changing R alone. The beaming is also sensitive to local time dilation at the NS surface, which is in turn sensitive to the compactness (M/R). The pulse profile thus yields a statistical constraint on M and R.

Naturally, there are additional model parameters affecting the pulse profile, which must be properly marginalised over when statistically inferring M and R. These include the specific details of local comoving radiation field (in angular space and energy space) and a priori unknown geometrical factors (the hot-spot size, shape, and inclination $\theta$; observer inclination $i$; and emission from the rest of the star and disk, which may also exhibit pulsations). However, the resulting degeneracies can be broken, allowing successful recovery of M and R (Lo et al., 2013; Psaltis et al., 2014; Miller & Lamb, 2015). Knowledge of the geometrical factors (enabled by the polarimetry capabilities of eXTP) improves the situation still further.

Radiation coming from the hotspots is expected to be linearly polarised because the opacity is dominated by electron scattering (Viironen & Poutanen, 2004). Both the observed polarization degree (PD) and polarization angle (PA) change with the rotational phase $\phi$ following variations of the angle the spot is observed and of the projection angle of the hotspot normal on the sky (see Fig. 6) The variation of PA $\chi$ can be well described by the

[1]The Schwarzschild exterior spacetime is only approximate for rotating compact stars. The mathematical structure of both the interior and exterior spacetime of a spinning NS is well understood in general relativistic gravity; high-accuracy spacetimes for rapidly spinning NSs can be computed numerically, albeit expensively (for a review see Stergioulas, 2003). For families of EOS, there exist (numerically computed) approximate universalities relating first-order (and higher) spacetime structure and the axisymmetric (oblate) coordinate surface of the star to low-order properties – specifically, the mass monopole moment, the equatorial coordinate radius, and the coordinate spin frequency (see for exampe the review of Yagi & Yunes, 2016). In order to simulate the observable radiation for the application of statistical inference, various approximations are employed which which demonstrably reduce computation time. Given such a universal relation, one typically embeds an oblate surface from which radiation emanates in an exterior spacetime, and either (i) exploits spherical symmetry of the exterior (Schwarzschild) solution (see for example Morsink et al., 2007), or (ii) permits axisymmetry, but neglects structure beyond second-order in a metric expansion in terms of a natural variable (see for example Bauböck et al., 2012, and references therein). The accuracy of these approximations are well understood (see the extensive discussion in Watts et al., 2016): employing a Schwarzschild exterior spacetime introduces systematic errors in the pulse profile on the order of several percent for a neutron star spinning at several hundred Hz. Statistical uncertainty incurred due to noise in eXTP observations is expected to dominate systematic biases which would arise from such exterior spacetime approximation.

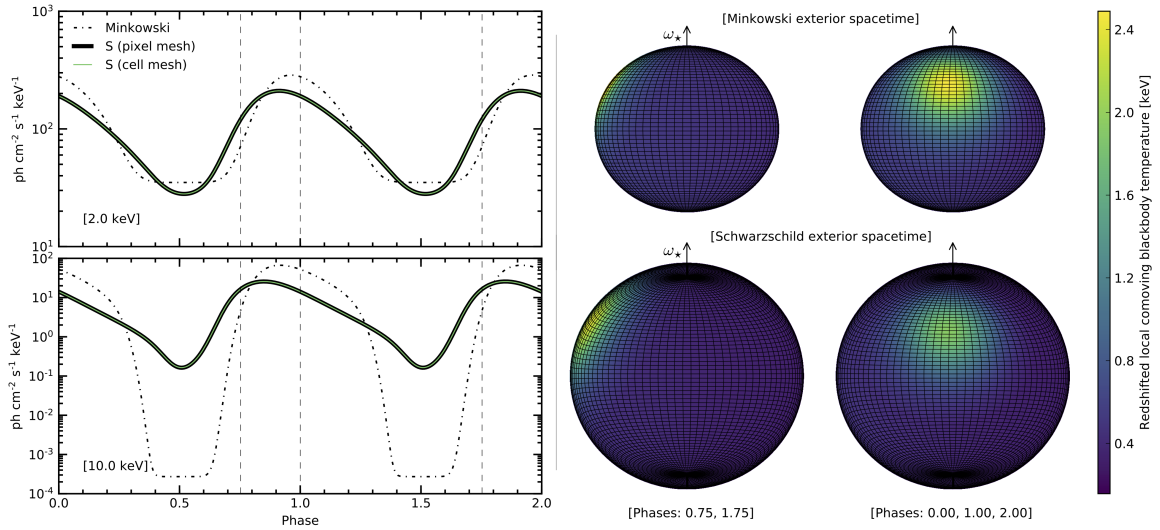


Figure 4: **Stellar rotation modulates emission from a hot region ('hot-spot'), generating an X-ray pulsation. Relativistic effects encode information about M and R in the normalisation and harmonic content of the pulse profile. These effects are key observables exploited by the pulse profile modelling technique, and include Doppler boosting and gravitational redshifting, time-delays, and light bending (which renders the far side of the star partially visible). The Figure illustrates these effects for a rapidly spinning, oblate star.** The figure compares pulse profiles computed with a flat Minkowski *exterior* spacetime to those computed with a realistic Schwarzschild exterior spacetime[1]. We use: a gravitational mass of 1.8 $M_\odot$; an equatorial coordinate radius of 14 km; a coordinate spin frequency of 600 Hz; and a distance of 0.2 kpc Figure to be updated to a distance of 2 kpc, more appropriate for accretion-powered pulsars.. The local photospheric radiation field is completely specified by the local comoving blackbody temperature. The temperature field is non-evolving in a coordinate chart which corotates with the photosphere, and is constituted by a hot-spot with an angular radius of 60°, centred at a colatitude of 60°. Its temperature falls smoothly from 2.5 keV at the centre to 0.5 keV at the boundary, where the latter is the temperature elsewhere. All computations are done using the X-PSI code suite (Riley et al. in prep), which employs two independent algorithms for integrating the incident radiation field. One discretises the photosphere with a moving *cell* mesh; the other discretises the image-plane with a static *pixel* mesh. Left: Monochromatic profiles at two energies (2 and 10 keV), for two exterior spacetimes. Right: The resolved stellar photosphere at two rotational phases. The colour corresponds to the redshifted temperature at the image-plane.

rotating vector model (Radhakrishnan & Cooke, 1969):

$$\tan\chi = -\frac{\sin\theta\ \sin\phi}{\sin i\ \cos\theta - \cos i\ \sin\theta\ \cos\phi}. \tag{1}$$

This formula can be corrected for the rapid rotation (Ferguson, 1973, 1976) and gravitational light bending, but the effect is not negligible only for spins in excess of 500 Hz (Viironen & Poutanen, 2004). The phase-dependence of PA allows to constrain both angles $i$ and $\theta$.

## 2.2 Accretion-powered millisecond pulsars

Cross-check final estimates with Simulations Working Group.

Accretion-powered millisecond pulsars (AMPs) contain weakly magnetised neutron stars (with $B \sim 10^8 - 10^9$ G accreting matter from a typically rather small companion star (Patruno & Watts, 2012). More than a dozen sources are known at present, all transients that go into outbursts every few years. Neutron stars in these systems have been spun by accretion up to the millisecond periods. Close to the neutron star, the accreting matter follows the magnetic field lines hitting the surface close to the magnetic poles. The resulting shockwave heats the

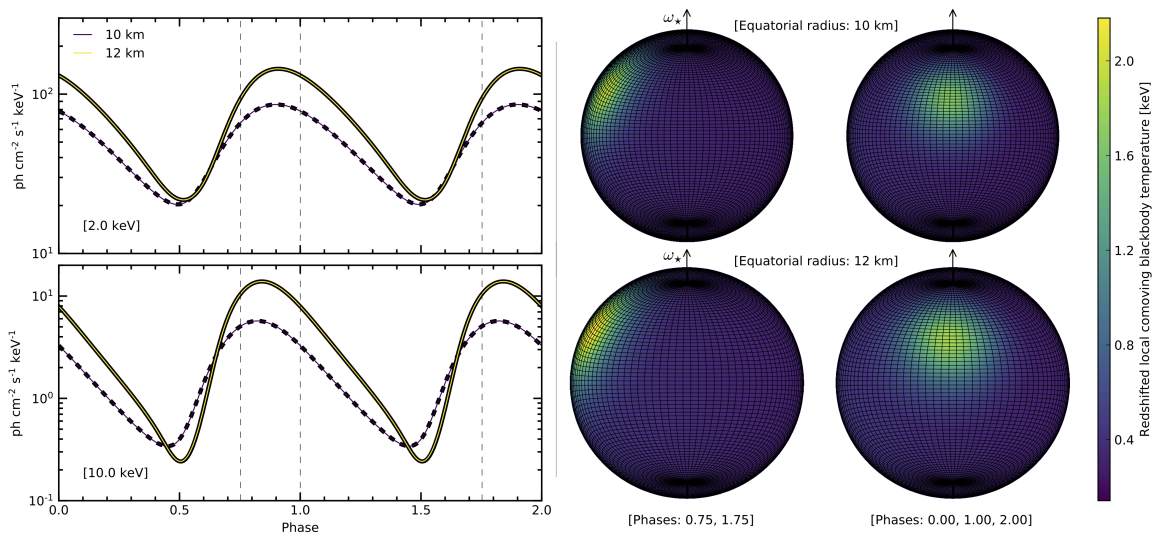


Figure 5: The Figure illustrates the effect of changing the equatorial radius on the monochromatic pulse profiles, whilst all other parameters are held constant at the values implemented in Figure 4. We use the realistic exterior spacetime described in Figure 4. The two synthetic stars shown are of equal gravitational mass and spin frequency, but have equatorial radii of 10 km and 12 km; these stars require distinct EOS models to exist. The pulse profiles are clearly sensitive to the equatorial radius, and it is the need to detect these differences that drive the design requirements for eXTP.

electrons to ~30–60 keV producing X-ray radiation by thermal Comptonization in a slab of Thomson optical depth of order unity (Poutanen, 2008). Rotation of the hotspot causes modulation of the observed flux with the pulsar phase as a result of changing projected area as well as of Doppler boosting. As the observed pulsations indicate that the shock covers only a small part of the neutron star surface, the scattered radiation should be linearly polarized up to 20%, depending on the pulse phase, the photon energy and the geometry of the system. In addition to the emission from the shock, pulsating thermal emission from the heated neutron star surface is seen at lower energies. In the peaks of the outbursts, when the accretion rate is high, the pulse profiles are usually very stable and rather sinusoidal with a harmonic content growing towards higher energies as a result of stronger contribution of the Comptonized emission which has more anisotropic emission pattern. The pulse shape implies that only a single hotspot is seen, while the secondary pole is blocked by the accretion disk. The pulse stability allows the collection of millions of photons under constant conditions.

One of the challenges for modelling pulse profiles from AMPs is the absence of first-principles models that predict the emission pattern from the shock. The angular dependence, therefore, has to be parametrised, based on models of radiation transfer in an optically thin slab of hot electrons. Degeneracy between the number of parameters did not allow strong constraints on M and R from RXTE data (Poutanen & Gierliński, 2003; Leahy et al., 2008, 2009, 2011). The LAD on eXTP would allow the collection of many more photons, and significant improvement in the constraints on M and R (see Fig. 7). Furthermore, in a 100 ks observation of a bright AMP such as SAX J1808.4–3654 or XTE J1751–305 the X-ray polarimeter onboard of eXTP can measure polarisation in 10 phase bins at the $3\sigma$ level and thus determine the basic geometrical parameters such as the inclinations of the spot and the observer (Fig. 6). This not only improves the constraints on M and R, but allows an independent check of the fitting procedure based on the pulse profile alone.

Observations with the LAD of the photospheric radius expansion bursts from the AMPs and analysis of their spectral evolution in the cooling tail give independent M–R constraints (see for example Suleimanov et al., 2011a; Poutanen et al., 2014; Nättilä et al., 2016) allowing us to put serious constraints on the EOS of cold dense matter (see dotted black curves in Fig. 7 and the resulting M–R error box).

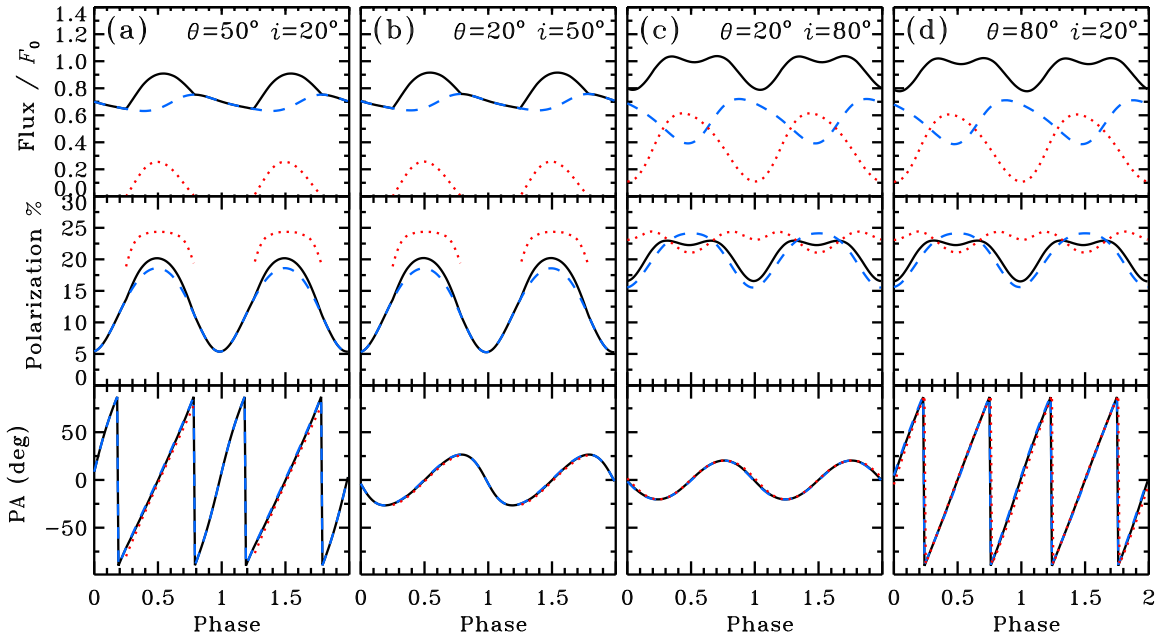


Figure 6: The pulse profile as well as the phase-dependence of the PD and PA. Black solid line give the contribution of two antipodal spots, while the dashed and dotted line correspond to the contribution of each spot separately. The pulse profile and PD are degenerate to exchanging $i$ and $\theta$, while the PA shows dramatically different behaviour allowing both angles to be obtained (adapted from Viironen & Poutanen, 2004).

## 2.3 Burst oscillation sources

Hotspots that form during thermonuclear explosions on accreting NS give rise to pulsations known as burst oscillations (for reviews see Strohmayer & Bildsten, 2006; Galloway et al., 2008; Watts, 2012). Burst oscillation sources are particularly attractive for M-R measurement in that they are numerous (increasing the odds of sampling a range of masses), have a well-understood thermal spectrum (Suleimanov et al., 2011b; Miller et al., 2013b), and offer multiple opportunities for independent cross-checks using complementary constraints (Bhattacharyya et al., 2005; Chang et al., 2005; Lo et al., 2013), thereby reducing systematic errors . Detailed studies have shown that accuracies of a few % in M and R can be obtained with $10^6$ pulsed photons (Lo et al., 2013; Psaltis et al., 2014; Miller & Lamb, 2015). In addition the technique is robust, with clear flags if any of the assumptions made during the fitting process are breached.

To estimate the observing time required for known sources we can use the burst oscillation amplitude, burst recurrence times and the percentage of bursts with oscillations observed by RXTE . For the persistent burst oscillation sources 4U 1636-536 and 4U 1728-34 we would require 350 ks and 375 ks respectively. For burst oscillations from the transient AMPs SAX J1808.4-3658 and XTE J1814-338 we would require 490 ks and 275 ks respectively. These observing times are substantial, but feasible. Burst oscillations from AMPs are particularly useful since the M-R measurements they generate can be compared to the results obtained from pulse profile fitting of accretion powered pulsations from the same sources (Sect. 2.2). . In addition the constraints on system geometry (inclination) acquired from the phase-dependence of the polarization of the persistent emission can also be used in fitting the burst oscillations, reducing uncertainties on M and R. Additional constraints for burst oscillation sources will also come from spectral fitting of strong bursts showing photospheric radius expansion (see Sect. 2.2).

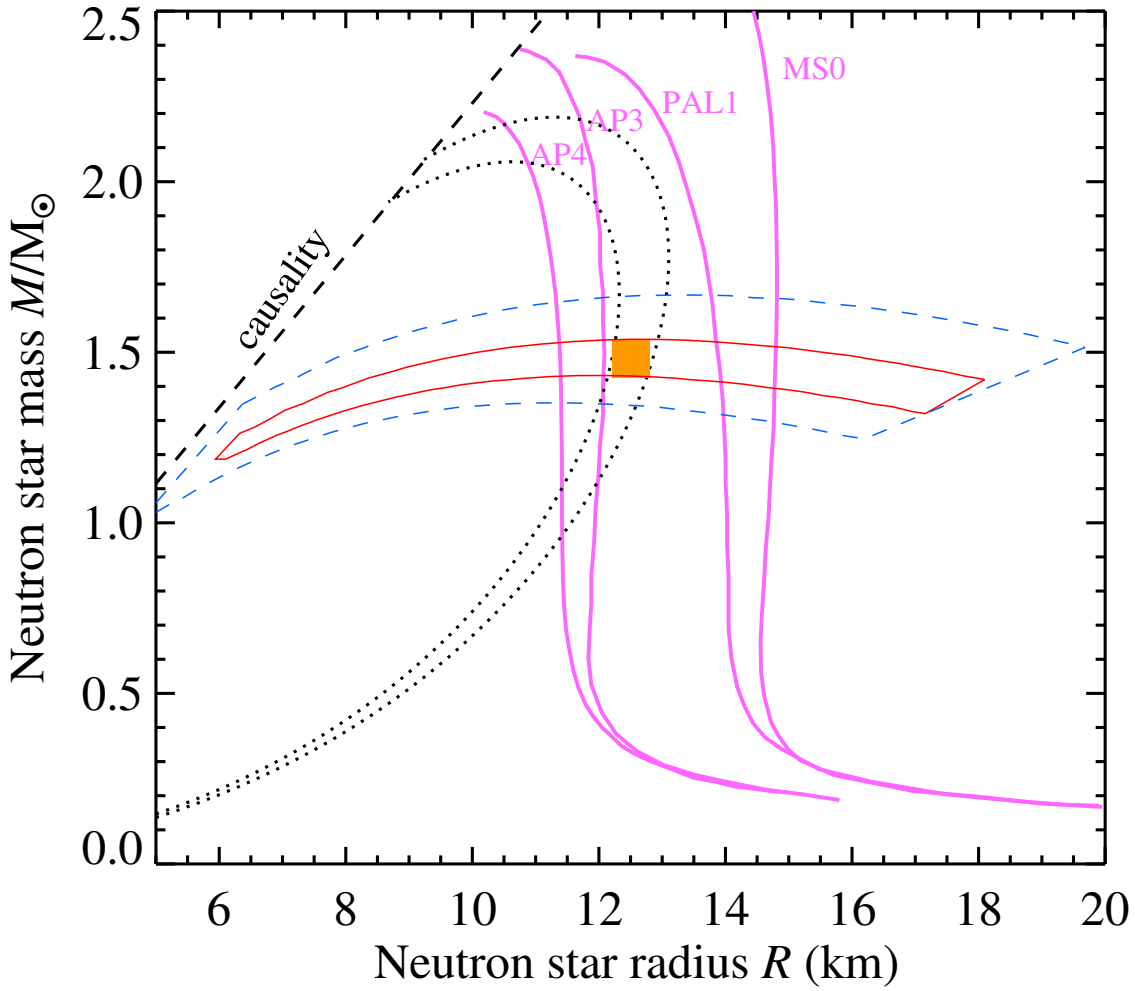


Figure 7: Constraints on M and R from the pulse profiles of AMP SAX J1808.4–3658 coming from the RXTE data (Poutanen & Gierliński, 2003) are shown by blue dashed contour, while the similar constraints given by LAD/eXTP are shown by the red solid contour. Spectral evolution during photospheric radius expansion bursts as determined using the cooling tail method (Suleimanov et al., 2011a) produce nearly perpendicular constraints on M and R given by dotted curves. The pink solid curves corresponds to different equations of state of cold dense matter. This figure to be updated to use same EOS models as in Figure 3 and Figure 8

## 2.4 Rotation-powered pulsars

NICER-SEXTANT (Arzoumanian et al., 2014) is a NASA Explorer Mission of Opportunity soft X-ray detector that was installed on the International Space Station in mid-2017. NICER applies the pulse profile modelling technique to rotation-powered X-ray pulsars (Bogdanov et al., 2008). Since NICER's targets rotate relatively slowly, it cannot rely on well-understood Doppler effects to break degeneracies between M and R (Psaltis et al., 2014). However if the surface pattern and mass of the neutron star are known a priori, NICER could in principle achieve an accuracy of ~ 2 % in R (Gendreau et al., 2012; Bogdanov, 2013). The mass is now known to 5% accuracy for NICER's primary target, PSR J0437-4715, but is not yet known for its other main targets. The surface pattern depends on the pulsar mechanism and is at present not well constrained, although theoretical work to address this topic is underway. NICER will have a peak effective area at 1 keV of about 2000 $cm^2$. eXTP will be a factor of a few larger in the soft waveband, enabling it to measure the energy-resolved pulse waveform

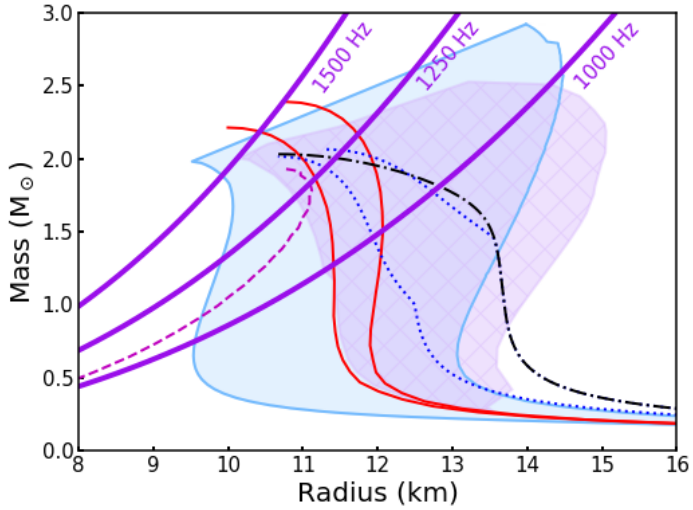


Figure 8: Spin limits on the EOS. The mass-shedding imit can be recast as an upper limit on radius for a star of a given spin rate (Haensel et al., 2009). This means that NS of a given spin rate must extend to the left of the relevant limit in the M-R plane (shown as thick violet lines, for various spins). EOS models as in Figure 3. The current record holder, which spins at 716 Hz (Hessels et al., 2006) is not constraining. However given a high enough spin individual EOS can be ruled out. Above 1000 Hz, for example, some individual EOS in the pQCD band would be excluded.

of pulsars such as PSR J0437-4715 more efficiently than NICER-SEXTANT. This opens up the prospect of taking observations of fainter sources, should promising targets be identified.
Still to be added (work in progress, to be completed by mid October)- results of simulations indicating what eXTP will be able to achieve for these sources compared to NICER.

## 3 Spin measurement

NS with the fastest spins constrain the EOS since the limiting spin rate, at which the equatorial surface velocity is comparable to the local orbital velocity and mass-shedding occurs, is a function of M and R (Figure 8). Softer EOS have smaller R for a given M, and hence have higher limiting spin rates. More rapidly spinning neutron stars place increasingly stringent constraints on the EOS. The current record holder, a millsecond radio pulsar (MSP) spinning at 716 Hz (Hessels et al., 2006), does not rotate rapidly enough to rule out any EOS models. However the discovery of a NS with a sub-millisecond spin period would place a strong and clean constraint on the EOS. There are prospects for finding more rapidly spinning neutron stars in future radio surveys (Watts et al., 2015), however since the standard formation route for the MSPs is via spin-up due to accretion (Alpar et al., 1982; Radhakrishnan & Srinivasan, 1982; Bhattacharya & van den Heuvel, 1991), it is clear that we should look in the X-ray as well as the radio, and theory has long suggested that accretion could spin stars up close to the break-up limit (Cook et al., 1994). Interestingly the drop-off in spin distribution at high spin rates seen in the MSP sample is not seen in the current (albeit much more limited) sample of accreting neutron stars (Watts et al., 2016).

Since eXTP would have a larger effective area than all preceding X-ray timing missions, it is well suited to discover many more NS spins, using both burst oscillations and accretion-powered pulsations. We know from RXTE that the latter can be highly intermittent (Galloway et al., 2007; Casella et al., 2008; Altamirano et al., 2008), perhaps due to the way that accretion flows are channeled onto weakly magnetized NS (Romanova et al., 2008), or because these systems are close to alignment (Lamb et al., 2009). In addition, weak persistent pulsations are expected in systems where magnetic field evolution as accretion progresses has driven the system towards alignment (Ruderman, 1991). Searches for weak pulsations can exploit the sophisticated semi-coherent techniques being used for the Fermi pulsar surveys (Atwood et al., 2006; Abdo et al., 2009; Messenger, 2011; Pletsch et al., 2012), which compensate for orbital Doppler smearing.

eXTP will be able to detect burst oscillations in individual Type I X-ray bursts to amplitudes of 0.4 % (1.3%)

rms in the burst tail (rise); by stacking bursts sensitivity improves. In estimating detectability of accretion-powered pulsations with eXTP we consider three source classes: bright (e.g. Sco X-1), moderate (e.g. Aql X-1) and faint (e.g. XTE J1807-294). We consider both coherent and semi-coherent searches. Coherent searches consider a simple FFT in a short data segment so that we do not lose coherence of the signal as a consequence of Doppler shifts induced by the orbital motion. We consider a duration of 128s, comparable to the duration of intermittent pulsation episodes seen in Aql X-1 (Casella et al., 2008). Under these assumptions, eXTP will be able to perform a coherent search for intermittent pulsations down to amplitudes of 0.04 % (bright), 0.3% rms (moderate), 1.9% rms (faint) (5 $\sigma$ single trial limits).

For semi-coherent searches, we assume a 10 ks long observation, which need not be continuous, and coherence lengths (the segment over which we can search for individual trains of coherent pulsations) of 256s and 512s. These assumptions are extremely conservative, and we would expect to be able to do better than this for many of our target sources, for which we know orbital parameters, reducing the number of templates to be searched. For this type of search eXTP would be sensitive down to amplitudes of 0.01% rms (bright), 0.1 % rms (moderate), and 0.6 % rms (faint) (5 $\sigma$ single trial limits).

## 4 Constraints from accretion flows in the disks of NS LMXBs

The advanced timing and polarimetry capabilities of eXTP will also enable other methods that could constrain the EOS for accreting neutron stars. The methods outlined in this section are derived from phenomena associated with the inner parts of the accretion disk. Compared to the spin rate constraint described in Section 3 they are more model-dependent. However they are nonetheless powerful as they provide additional complementary cross-checks and allow us to calibrate different techniques to extend our reach to a wider range of sources.

### 4.1 Kilohertz Quasi-Periodic Oscillations (QPOs)

Kilohertz QPOs are rapid variations in the intensity of neutron star LMXBs, both persistent and transient (see van der Klis, 2000, for a review). RXTE observed this phenomenon in a few tens of sources. The corresponding millisecond time scale is so short that the QPOs must be associated with dynamical time scales in the accretion flow in the vicinity of neutron star. In many cases, these QPOs are seen as twin peaks in the Fourier power spectra. If one of the twin peaks is an indicator of the orbital motion in the accretion flow, it would put a constraint on neutron star mass and radius: the stable orbit must be outside the neutron star and at its smallest at the innermost stable circular orbit (ISCO) (Miller et al., 1998).

In addition to the association of the kHz QPOs with orbital motion in the innermost accretion flow onto neutron stars based on the millisecond time scales, there is increasing observational evidence that the kHz QPOs do indeed indicate the orbital frequency in the accretion flow (or boundary layer) surrounding the neutron star. The frequency of the lower kHz QPOs is anti-correlated with the mHz QPO flux in 4U 1608-52, which is consistent with a modulation of the orbital frequency under radiation force from the neutron star (Yu & van der Klis, 2002). The pulse amplitude changes significantly when the upper kHz QPO passes the spin frequency in the accretion-powered millisecond pulsar SAX J1808-3654, strongly suggesting that the QPO is produced by azimuthal motion at the inner edge of the accretion disk, most likely orbital motion (Bult & van der Klis, 2015).

The behaviour of the QPOs as they approach their highest frequencies was difficult to resolve with RXTE as both amplitude and coherence drop at this point, although the behaviour is consistent with that expected near the ISCO (Barret et al., 2006). eXTP will make breakthroughs by being able to track the QPOs to higher frequencies despite the weaker amplitudes, and investigate variability on shorter timescales. The latter is very important: QPOs in Sco X-1, for example, have been observed to drift by more than 22 Hz in 0.08s (Yu et al., 2001).

The QPO coherence drop and rapid frequency drifts may be due to radiation force effects on the orbital frequency in the accretion flow, since an anti-correlation between the kHz QPO frequency and the X-ray flux were detected on the time scales of lower frequency QPOs where the flux probably originates from the neutron

star (Yu et al., 2001; Yu & van der Klis, 2002). In sources with the most detections of kHz QPOs such as 4U 1636-53, the maximum QPO frequency seems to be anti-correlated with the X-ray flux (Barret et al., 2005). Both this anti-correlation and the QPO coherence variation can be explained by radiation force effects. This in turn can put constraints on NS EOS by measurements of the maximum kHz QPO frequency and the X-ray flux (Yu, 2008), although GRMHD simulations with radiation will be needed to create models of sufficient accuracy.

WIth eXTP, the maximum kHz QPO frequency measured in bright sources on short time scales, and in sources at lower flux levels, would increase by about 50 Hz (or 5%). Using the ISCO model of Miller et al. (1998), this would lower the upper limit on NS radius by ~0.5 km or the mass by $\sim 0.1 M_{\odot}$. Corrections for radiation force effects would modify these estimates somewhat.

### 4.2 Constraints from relativistic Fe line modelling

A broad relativistic Fe K$\alpha$ spectral emission line is observed from many stellar-mass and supermassive black hole systems (Fabian et al., 2000; Reynolds & Nowak, 2003; Miller, 2007). Such a fluorescent line near 6 keV is believed to be generated by the reflection of hard X-rays from the accretion disk, and is shaped by various physical effects, such as the Doppler effect, special relativistic beaming, gravitational redshift and general relativistic light-bending. The shape and energies of this line can be used to measure $r_{\rm in}c^2/GM$, i.e., the inner-edge radius $r_{\rm in}$ of the accretion disk in the unit of the black hole mass $M$. By considering the disk inner-edge to be the innermost stable circular orbit (ISCO), which may be a reasonable assumption for black holes, one can infer the black hole angular momentum parameter $a$ for the Kerr spacetime.

A broad relativistic spectral line has also been observed from a number of neutron star LMXBs (Bhattacharyya & Strohmayer, 2007; Cackett et al., 2008; Pandel et al., 2008; D'Aì et al., 2009; Cackett et al., 2010; Miller et al., 2013a; Chiang et al., 2016) . As for black holes, one can infer $r_{\rm in}c^2/GM$ for neutron stars from the relativistic Fe line. Since the disk inner edge radius $r_{\rm in} \geq R$, the inferred $r_{\rm in}c^2/GM$ provides an upper limit on $Rc^2/GM$. One can therefore use $M - r_{\rm in}c^2/GM$ space (instead of $M - R$ space) for a known $\nu_{\rm spin}$ value to constrain EOS models (Figure 9). This method requires computations of $r_{\rm in}c^2/GM$ for given $M$ and $\nu$ values and EOS models. Note that, while $r_{\rm in} = r_{\rm ISCO}$ (i.e., ISCO radius) for a black hole, $r_{\rm in}$ is either $r_{\rm ISCO}$ or $R$, whichever is greater, for a neutron star. For a spinning (Kerr) black hole, $r_{\rm ISCO}$ can be analytically computed as a function of $M$ and $a$. For a neutron star in an LMXB, one must compute $r_{\rm ISCO}$ and $R$ values numerically for various EOS models and neutron star configurations, using an appropriate rapidly spinning stellar spacetime. Simulations for the eXTP LAD show that a statistical error of less than 0.1 in $r_{\rm in}c^2/GM$, sufficient to distinguish models, is achievable with a 30 ks exposure (Figure 9).

## 5 Summary

eXTP offers unprecedented discovery space for the EOS of supranuclear density matter, by enabling precision measurements of neutron star mass and radius. The combination of large area and polarimeter will enable pulse profile modelling of accretion-powered pulsations. For a number of sources we expect to be able to obtain complementary and completely independent measurements using pulse profile modelling of burst oscillations, and spectral modelling of photospheric radius expansion bursts. eXTP's large area would also enable us to understake the most sensitive searches for accretion-powered pulsations and burst oscillations yet undertaken. Both yield the spin frequency of the neutron star. A single measurement of sub millisecond period spin would provide a clean and extremely robust constraint on the EOS. Being able to apply multiple independent techniques to the same sources will enable us to combat any systematic or modelling errors.

## References

Abdo A.A., Ackermann M., Ajello M., et al., 2009, Science 325, 840

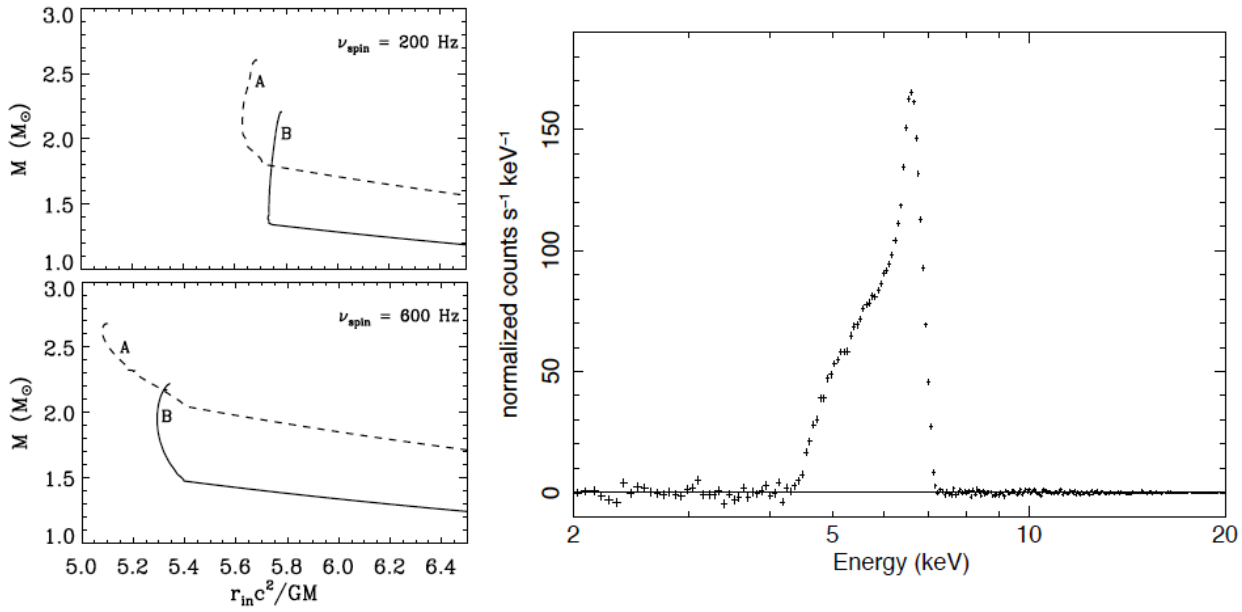


Figure 9: EOS constraints from relativistic Fe line modelling. Left panel ( adapted from Bhattacharyya, 2011): $M$ versus $r_{\rm in}c^2/GM$ curves for two reasonable values of $\nu$ and for two currently viable EOS models: one hard (A) and one soft (B). On the straight (near horizontal) portions, $r_{\rm in} = R$; elsewhere $r_{\rm in} = r_{\rm ISCO}$. Since the geometrically thin accretion disk, which gives rise to the broad relativistic line, may be truncated by radiation pressure or a stellar magnetic field at a radius larger than $r_{\rm ISCO}$ and $R$, the observationally inferred $r_{\rm in}c^2/GM$ is an upper limit. If $M$ can be measured independently (e.g. by one of the other methods described in this white paper), this upper limit on $r_{\rm in}c^2/GM$ provides an extra constraint on the EOS. In addition, if the upper limit of $r_{\rm in}c^2/GM$ is sufficiently small, softer EOS models can be ruled out without a mass measurement. Right: Simulated relativistic Fe line spectrum for a 30ks observation with eXTP (residual plot). We assume a `wabs(bbody+diskbb+powerlaw+diskline)` XSPEC model with reasonable values of $2-20$ keV flux ($6.4\times10^{-9}$ erg cm$^2$ s$^{-1}$) and line equivalent width (124 eV).


Acernese F., Agathos M., Agatsuma K., et al., 2015, Classical and Quantum Gravity 32, 024001

Agathos M., Meidam J., Del Pozzo W., et al., 2015, Physical Review D 92, 023012

Akmal A., Pandharipande V.R., 1997, Phys. Rev. C 56, 2261

Alpar M.A., Cheng A.F., Ruderman M.A., Shaham J., 1982, Nature 300, 728

Altamirano D., Casella P., Patruno A., et al., 2008, ApJ 674, L45

Antoniadis J., Freire P.C.C., Wex N., et al., 2013, Science 340, 448

Arzoumanian Z., Gendreau K.C., Baker C.L., et al., 2014, In: Society of Photo-Optical Instrumentation Engineers (SPIE) Conference Series, Vol. 9144. Society of Photo-Optical Instrumentation Engineers (SPIE) Conference Series, p. 20

Atwood W.B., Ziegler M., Johnson R.P., Baughman B.M., 2006, ApJ 652, L49

Barret D., Olive J.F., Miller M.C., 2005, MNRAS 361, 855

Barret D., Olive J.F., Miller M.C., 2006, MNRAS 370, 1140

Bauböck M., Berti E., Psaltis D., Özel F., 2013, ApJ 777, 68

Bauböck M., Psaltis D., Özel F., Johannsen T., 2012, ApJ 753, 175

Bauswein A., Janka H.T., Hebeler K., Schwenk A., 2012, Phys. Rev. D 86, 063001

Bauswein A., Stergioulas N., Janka H.T., 2014, Phys. Rev. D 90, 023002

Bednarek I., Haensel P., Zdunik J.L., et al., 2012, A&A 543, A157

Bhattacharya D., van den Heuvel E.P.J., 1991, Physics Reports 203, 1

Bhattacharyya S., 2011, MNRAS 415, 3247

Bhattacharyya S., Miller M.C., Lamb F.K., 2005, In: Smith R. (ed.) X-ray Diagnostics of Astrophysical Plasmas: Theory, Experiment, and Observation, Vol. 774. American Institute of Physics Conference Series, p.291

Bhattacharyya S., Strohmayer T.E., 2007, ApJ 664, L103

Bogdanov S., 2013, ApJ 762, 96

Bogdanov S., Grindlay J.E., Rybicki G.B., 2008, ApJ 689, 407

Bult P., van der Klis M., 2015, ApJ 806, 90

Cackett E.M., Miller J.M., Ballantyne D.R., et al., 2010, ApJ 720, 205

Cackett E.M., Miller J.M., Bhattacharyya S., et al., 2008, ApJ 674, 415

Cadeau C., Morsink S.M., Leahy D., Campbell S.S., 2007, ApJ 654, 458

Casella P., Altamirano D., Patruno A., et al., 2008, ApJ 674, L41

Chang P., Bildsten L., Wasserman I., 2005, ApJ 629, 998

Chatziioannou K., Yagi K., Klein A., et al., 2015, Phys. Rev. D 92,

104008
Chiang C.Y., Cackett E.M., Miller J.M., et al., 2016, ApJ 821, 105
Clark J.A., Bauswein A., Stergioulas N., Shoemaker D., 2016, Classical and Quantum Gravity 33, 085003
Cook G.B., Shapiro S.L., Teukolsky S.A., 1994, ApJ 423, L117
D'Aì A., Iaria R., Di Salvo T., et al., 2009, ApJ 693, L1
Del Pozzo W., Li T.G.F., Agathos M., et al., 2013, Physical Review Letters 111, 071101
Demorest P.B., Pennucci T., Ransom S.M., et al., 2010, Nature 467, 1081
Fabian A.C., Iwasawa K., Reynolds C.S., Young A.J., 2000, PASP 112, 1145
Favata M., 2014, Physical Review Letters 112, 101101
Ferguson D.C., 1973, ApJ 183, 977
Ferguson D.C., 1976, ApJ 205, 247
Galloway D.K., Morgan E.H., Krauss M.I., et al., 2007, ApJ 654, L73
Galloway D.K., Muno M.P., Hartman J.M., et al., 2008, ApJ Supp. 179, 360
Gendreau K.C., Arzoumanian Z., Okajima T., 2012, In: Society of Photo-Optical Instrumentation Engineers (SPIE) Conference Series, Vol. 8443. Society of Photo-Optical Instrumentation Engineers (SPIE) Conference Series, p. 13
Guillot S., Rutledge R.E., 2014, ApJ 796, L3
Haensel P., Zdunik J.L., Bejger M., Lattimer J.M., 2009, A&A 502, 605
Hebeler K., Lattimer J.M., Pethick C.J., Schwenk A., 2013, ApJ 773, 11
Hessels J.W.T., Ransom S.M., Stairs I.H., et al., 2006, Science 311, 1901
Hotokezaka K., Kyutoku K., Sekiguchi Y.i., Shibata M., 2016, Phys. Rev. D 93, 064082
Kramer M., Wex N., 2009, Classical and Quantum Gravity 26, 073001
Kurkela A., Fraga E.S., Schaffner-Bielich J., Vuorinen A., 2014, ApJ 789, 127
Lackey B.D., Kyutoku K., Shibata M., et al., 2014, Phys. Rev. D 89, 043009
Lackey B.D., Wade L., 2015, Physical Review D 91, 043002
Lamb F.K., Boutloukos S., Van Wassenhove S., et al., 2009, ApJ 705, L36
Lattimer J.M., Prakash M., 2001, ApJ 550, 426
Leahy D.A., Morsink S.M., Cadeau C., 2008, ApJ 672, 1119
Leahy D.A., Morsink S.M., Chou Y., 2011, ApJ 742, 17
Leahy D.A., Morsink S.M., Chung Y.Y., Chou Y., 2009, ApJ 691, 1235
Lindblom L., 1992, ApJ 398, 569
Lo K.H., Miller M.C., Bhattacharyya S., Lamb F.K., 2013, ApJ 776, 19
Messenger C., 2011, Phys. Rev. D 84, 083003
Miller J.M., 2007, Ann. Rev. Astron. Astrophys. 45, 441
Miller J.M., Parker M.L., Fuerst F., et al., 2013a, ApJ 779, L2
Miller M.C., 2013, ArXiv e-prints
Miller M.C., Boutloukos S., Lo K.H., Lamb F.K., 2013b, In: Zhang C.M., Belloni T., Méndez M., Zhang S.N. (eds.) IAU Symposium, Vol. 290. IAU Symposium, p.101
Miller M.C., Lamb F.K., 1998, ApJ 499, L37
Miller M.C., Lamb F.K., 2015, ApJ 808, 31
Miller M.C., Lamb F.K., Psaltis D., 1998, ApJ 508, 791
Morsink S.M., Leahy D.A., Cadeau C., Braga J., 2007, ApJ 663, 1244
Motch C., Wilms J., Barret D., et al., 2013, ArXiv e-prints
Nättilä J., Steiner A.W., Kajava J.J.E., et al., 2016, A&A 591, A25
Özel F., 2013, Reports on Progress in Physics 76, 016901
Özel F., Psaltis D., 2009, Phys. Rev. D 80, 103003
Pandel D., Kaaret P., Corbel S., 2008, ApJ 688, 1288
Patruno A., Watts A.L., 2012, ArXiv e-prints
Pechenick K.R., Ftaclas C., Cohen J.M., 1983, ApJ 274, 846
Pletsch H.J., Guillemot L., Allen B., et al., 2012, ApJ 744, 105
Poutanen J., 2008, In: Wijnands R., Altamirano D., Soleri P., Degenaar N., Rea N., Casella P., Patruno A., Linares M. (eds.) American Institute of Physics Conference Series, Vol. 1068. American Institute of Physics Conference Series, p.77
Poutanen J., Beloborodov A.M., 2006, MNRAS 373, 836
Poutanen J., Gierliński M., 2003, MNRAS 343, 1301
Poutanen J., Nättilä J., Kajava J.J.E., et al., 2014, MNRAS 442, 3777
Prakash M., Cooke J.R., Lattimer J.M., 1995, Phys. Rev. D 52, 661
Psaltis D., Özel F., 2014, ApJ 792, 87
Psaltis D., Özel F., Chakrabarty D., 2014, ApJ 787, 136
Radhakrishnan V., Cooke D.J., 1969, Astrophysics Letters 3, 225
Radhakrishnan V., Srinivasan G., 1982, Current Science 51, 1096
Read J.S., Baiotti L., Creighton J.D.E., et al., 2013, Phys. Rev. D 88, 044042
Read J.S., Lackey B.D., Owen B.J., Friedman J.L., 2009, Phys. Rev. D 79, 124032
Reynolds C.S., Nowak M.A., 2003, Physics Reports 377, 389
Romanova M.M., Kulkarni A.K., Lovelace R.V.E., 2008, ApJ 673, L171
Ruderman M., 1991, ApJ 366, 261
Steiner A.W., Heinke C.O., Bogdanov S., et al., 2017, ArXiv e-prints
Steiner A.W., Lattimer J.M., Brown E.F., 2013, ApJ 765, L5
Stergioulas N., 2003, Living Reviews in Relativity 6, 3
Strohmayer T., Bildsten L., 2006, New views of thermonuclear bursts, p.113
Suleimanov V., Poutanen J., Revnivtsev M., Werner K., 2011a, ApJ 742, 122
Suleimanov V., Poutanen J., Werner K., 2011b, A&A 527, A139
Takami K., Rezzolla L., Baiotti L., 2014, Physical Review Letters 113, 091104
The LIGO Scientific CollaborationAasi J., Abbott B.P., et al., 2015, Classical and Quantum Gravity 32, 074001
van der Klis M., 2000, ARAA 38, 717
Viironen K., Poutanen J., 2004, A&A 426, 985
Watts A., Espinoza C.M., Xu R., et al., 2015, Advancing Astrophysics with the Square Kilometre Array (AASKA14) 43
Watts A.L., 2012, Ann. Rev. Astron. Astrophys. 50, 609
Watts A.L., Andersson N., Chakrabarty D., et al., 2016, Reviews of Modern Physics 88, 021001
Yagi K., Yunes N., 2016, ArXiv e-prints
Yu W., 2008, In: Yuan Y.F., Li X.D., Lai D. (eds.) Astrophysics of Compact Objects, Vol. 968. American Institute of Physics Conference Series, p.215
Yu W., van der Klis M., 2002, ApJ 567, L67
Yu W., van der Klis M., Jonker P.G., 2001, ApJ 559, L29
Zdunik J.L., Haensel P., 2013, A&A 551, A61